Integrating observation and statistical forecasts over sub-Saharan Africa to support Famine Early Warning

Extended Asbtract

Chris Funk, Climate Hazard Group, Geography, Santa Barbara
James P. Verdin, United States Geological Survey
Greg Husak, Climate Hazard Group, Geography, Santa Barbara

Famine early warning in Africa presents unique challenges and rewards. Hydrologic extremes must be tracked and anticipated over complex and changing climate regimes. The successful anticipation and interpretation of hydrologic shocks can initiate effective government response, saving lives and softening the impacts of droughts and floods. While both monitoring and forecast technologies continue to advance, discontinuities between monitoring and forecast systems inhibit effective decision making. Monitoring systems typically rely on high resolution satellite remote-sensed normalized difference vegetation index (NDVI) and rainfall imagery. Forecast systems provide information on a variety of scales and formats. Non-meteorologists are often unable or unwilling to connect the dots between these disparate sources of information. To mitigate these problem researchers at UCSB's Climate Hazard Group, NASA GIMMS and USGS/EROS are implementing a NASA-funded integrated decision support system that combines the monitoring of precipitation and NDVI with statistical one-to-three month forecasts. We present the monitoring/forecast system, assess its accuracy, and demonstrate its application in food insecure sub-Saharan Africa.

1. Introduction

In southern and eastern Africa, coping effectively with climate extremes is similar in cost and impact to war. On half acre farms with hand tools and poor soil the world's poorest families struggle to eke out an existence each year. They often fail. Eight hundred million Africans face dramatic food shortages each year[1]. Hunger and poverty drive a cycle of deprivation accounting for more than half of all child deaths. The causes of hunger are legion: rapid rural population growth, poor agricultural practices, limited market access, crop subsidies in Europe and the U.S., poor governance and drought. Meteorology can help reduce the societal and environmental costs of hydrologic extremes by providing adequate early warning. The 1997/98 season, associated with a very strong El Niño and positive Indian Ocean Dipole Event (Saji et al., 1999) resulted in substantial drought and crop damage across southern Africa. Extremely warm northwest Indian Ocean sea surface temperatures (SSTs) contributed to dramatic flooding over the Greater Horn of Africa (GHA[2]). These extreme moisture conditions in turn contributed to an outbreak of Rift Valley Fever, a mosquito-borne disease affecting cattle. This outbreak resulted in a moratorium on cattle exports, decimating agro-pastoral communities. As we write this extended abstract, in October of 2006, the climate conditions are similar. In this

---

[1] Food and Agriculture Organization, 'Food Insecurity in the World', 2005.
[2] Tanzania, Rwanda, Burundi, Kenya, Uganda, Ethiopia, Djibouti, Somalia and Eritrea.

context of likely climatic extremes, this short paper sketches the science behind our work for the USAID funded Famine Early Warning System Network (FEWS NET). The crux of this work is the monitoring and forecasting of hydrologic extremes. Hydrologic early warning (HEW) combines hydro-climatology (A) with socioeconomic analysis (B) to provide effective advance notice of potential crises associated with drought, flood or disease (Figure 1). An appropriate policy/governance framework (C) can then allow for effective early action, potentially saving thousands of lives and millions of dollars. Effective hydro-climatology, in turn, requires accurate, up-to-date rainfall climatologies, easy-to-understand representations to decision makers and timely forecasts.

For eastern and southern Africa we have developed and implemented three solutions to address each of these three problems. The Improved Rainfall Estimation (IRE) technique combines topographically-enhanced grids of average rainfall with time-varying rainfall gauge and satellite estimates. This work is the latest (superior we believe) installment in our ongoing research into rainfall estimation in data sparse, topographically complex terrain (Funk et al., 2003; Funk and Michaelsen, 2004). These rainfall accumulations can then be fit with gamma distribution parameters (Husak et al., 2006) and expressed as standardized precipitation indices (SPI, McKee, 1993). Maps of SPI values typically range between -3 and 3. They retain their distribution characteristics across space and time. This characteristic facilitates their application as a decision making tool. These maps are most useful in *advance* of hydro-climatic shocks. To this end the third component of this article presents our matched filter regression based short-lag forecast system. This uses monthly fields of NCEP-NCAR reanalysis data (Kalnay et al., 1996) as the basis of statistical SPI forecasts. Pacific and Indian Ocean SSTs, Indian Ocean SSTs, and 200 and 500 hPa zonal and meridional winds over eastern and southern Africa are used as inputs. This statistical framework was used successfully to predict the poor late season rains in southern Africa during the 2002/03 El Niño (Funk et al., 2003; Magadzire et al., 2006), as well as the switch to positive rainfall anomalies during 2003/04. This work extends the application to gridded SPI values across all of eastern and southern Africa (ESEA, 0-55°E, 20°N-40°S).

This paper provides a brief introduction, methodological description, evaluation and discussion of each component. We conclude with a presentation of the 2006/07 November-December-January (NDJ) forecast, based on October 2006 data.

1.a The Improved Rainfall Estimation (IRE) Technique

The IRE technique combines traditional rainfall interpolation approaches with satellite-based precipitation surfaces. The approach has two objectives: i) make consistent (low-bias) estimates, ii) accurately. Similar to 'smart interpolation' approaches (Willmott and Matsura, 1995) commonly used to produce gridded fields (New et al. 1999, 2000), the IRE procedure is assisted by a long term mean field. In addition to the means, however, the IRE also incorporates satellite rainfall estimates. The recent decline in readily available high quality gauge data makes the use of satellite data critical, especially in many climatically and environmentally important areas of the developing world. While

our research has explored methods for using gravity wave based diagnostic models to improve satellite rainfall estimates (Funk and Michaelsen, 2004) and climatological rainfall time series (Funk et al., 2003), further analysis suggests that much of the complexities associated with orographic precipitation modeling at monthly and seasonal scales can be absorbed within sophisticated, topographically enhanced mean precipitation grids. These background fields can be used to remove the systematic bias commonly found in satellite precipitation fields. This procedure can also be used to introduce local variations into coarse precipitation surfaces. The unbiased satellite estimates, in turn, can in turn be combined with station data in a geostatistical framework.

1.b Standardized Precipitation Indices (SPI)

The Standardized Precipitation Index (SPI) is a method of presenting rainfall as a normalized variable (McKee, 1993). As a normalized variable, the SPI reports the probability of a rainfall event occurring, and therefore the practical significance of realizing a rainfall observation. This can represent an improvement over traditional methods such as percent-of-normal - which can inflate the significance of small anomalies during the dry season - and difference-from-normal - which does not reflect the typical variability in rainfall. The SPI can be created for any accumulation interval, allowing the SPI to be scaled to capture events of various duration, recognizing that short-term anomalies may be very different from long-term ones.

1.c Matched Filter Regression (MFR) short-lag forecasts

Recent advances in climate forecasting have demonstrated that statistical downscaling of global numerical weather prediction model fields can anticipate anomalous precipitation. Much of this research relies on the use of canonical correlation analysis to translate global climate model fields (i.e. 850 hPa winds) into target estimates. Much of this research relies on the use of canonical correlation analysis to translate global climate model fields (i.e. 850 hPa winds) into target estimates. CHG research has produced a similar statistical approach (matched filter regression, MFR) that focuses on a single predicted time-series (rather than a field, as in CCA). In remote sensing applications, matched filters can be used to quantify a weak signal against a noisy background (Funk et al., 1999). In climate applications matched filters are used to pre-scale multivariate predictors before applying traditional eigen-based analysis techniques. MFR has been used to successfully to anticipate a poor 2002/03 growing season in Southern Africa (Funk et al. 2003a) and the return to normal rainfall in the latter half Southern Africa's rainy season in 2003/04 (Funk et al. 2003c).

2. Data

Three data sources were combined to produce satellite enhanced mean fields: long term (1996-2005) long term monthly means derived from the Climate Prediction Center African Rainfall Climatology (ARC, Xie et al., 2002), USGS Hydro 1K (Gesch et al., 1999) slopes and elevation data resampled to the ARC 0.1° grid, and FAO climate normals. We demonstrate the method with two sets of satellite rainfall estimates, the 27 year Global Precipitation Climatology Project (GPCP, Huffman et al., 1995, 1997, Adler

et al., 2003) and the 10 year ARC over Africa. Time-series of station data were obtained by combining data from the Global Historical Climate Network (Peterson and Vose, 1997), FAO (2001) with data obtained from the Ethiopian Meteorological Service and Famine Early Warning System Network (FEWS NET) archives. Monthly data was used in all instances.

3. Methods

3.a IRE Methods

The Improved rainfall estimation procedure has three distinct steps: i) the creation of satellite-enhanced long term mean fields, ii) the combination of the these fields with time-varying satellite fields to produced unbiased time-varying estimates, and the iii) fusion of these time-varying satellite estimates with regional near-real time station data. The objective is to use all available sources of data to produce the highest quality rainfall fields possible.

3.a.i FCLIM long term average mean fields

The spatial monthly mean field modeling used moving window matched filter regression Funk and Michaelsen, 2004) to produce an 0.1° 'first guess' field. Three spatially explicit predictands were used: ARC mean precipitation ($\bar{a}$), ARC mean precipitation times slope ($\bar{a}s$), and ARC mean precipitation time elevation ($\bar{a}e$). The $\bar{a}s$ and $\bar{a}e$ terms represent slope and elevation driven orographic enhancement, which is assumed to be locally linearly related to the ARC mean $\bar{a}$. Exploratory data analysis confirmed this hypothesis, although systematic relationships between slope, elevation and ARC means varied substantially as a function of latitude, and to a lesser degree, longitude. Thus local matched filter regressions were carried out using a moving 7° (~700 km) window fit to a set of 6965 FAO climate normals (2001). This produced 12 monthly 0.1° grids of average rainfall. Block kriging was then used to interpolate the 6965 at-station anomalies to the same grid. The MFR estimates and kriged anomalies were combined yielding 12 monthly FEWS NET climatology fields (FCLIM). Panel A of Figure 2 shows the long-term (1950-1980) annual FCLIM totals for sub-Saharan Africa, together with the locations of the FAOCLIM 2.0 station normals.

3.a.ii Producing unbiased rainfall estimates

This step uses FCLIM means to reduce the bias within satellite estimates, and in the case of the GPCP, introduce higher resolution information. Unbiased rainfall estimates (u) can be produced by multiplying the observed satellite rainfall estimates (s), expressed as a ratio of the satellite estimate long term mean ($\bar{s}$) by the corresponding monthly FLIM field ($\bar{f}$).

$$u = (s + \varepsilon)(\bar{s} + \varepsilon)^{-1} \bar{f} \qquad\qquad \text{[eq. 1]}$$

Epsilon is a suitably small value (typically ~ 10-20 mm) chosen such that the satellite rainfall, expressed as a ratio, converges to 1.0 as $\bar{s} \to 0$.

3.a.iii Merging additional station data

In the real world, satellite rainfall estimates are often calibrated with less-than-ideal station observation datasets. Many stations, for example, are not integrated within the electronic geo-telecommunication network. Global or regional estimates often lack the fairly dense networks available at national scales. Since there are often additional stations available in not-far-from real time, it makes sense to merge stations with a background unbiased rainfall estimates. While many choices of algorithm are available, simplicity is often required in an operational environment. To this end we have developed a simple double-IDW (inverse distance weighting) correction tool. This tool merges stations and a rainfall estimate grid in two consecutive passes. In the first pass *ratios* between stations and satellite grids are calculated and interpolated. In the second pass the ratios are multiplied against the RFE and the arithmetic at-stations *differences* interpolated. This second pass handles instances when the UBRF is 0. The interpolated anomalies are limited by a weighting function based on the distance from the nearest neighbor. This weighting function forces the ratio and arithmetic difference fields to zero and one (respectively) as the distance from a location approaches a user-defined threshold (7° in this case). This simple approach incorporates some of the benefits of kriging, but without substantial user intervention.

3.b SPI Methods

The SPI compares observations against distribution parameters derived from historical rainfall. The observations may be station data, satellite-based estimates or modeled output. Distribution parameters are derived by fitting gamma distribution parameters to historical data (Husak, 2006). The SPI is created by calculating the cumulative probability of the observation derived from the cumulative distribution function described by the historical distribution parameters. This cumulative probability is then converted to a normalized variable. Observations should be derived in a fashion similar to the historical values such that a comparison of the two will result in meaningful SPI results. Any bias or variability difference will lead to shifts in SPI values or values which are more/less extreme than would be expected. The SPI is created by calculating the cumulative probability of the observation derived from the cumulative distribution function described by the historical distribution parameters. This cumulative probability is then converted to a normalized variable typically ranging from -3 to 3.

3.c MFR Methods

In general, we can arrange n temporal observations of m heterogeneous reanalysis or numerical weather prediction variables in a m x n matrix defining our climate state, **X**. We can then transform each row **x** of **X** so that it has a mean of zero and an expected standard deviation equal to its correlation ($\mathbf{r_{x,w}}$) with our desired time series (**v**):

$$\mathbf{x}'_i = r_{\mathbf{x},v}\left(\mathbf{x}_i - \overline{\mathbf{x}}\right)\sigma_{\mathbf{x}}^{-1}, \forall i \in [1..n] \qquad [2]$$

Applying this transform to all the rows of **X** gives us a transformed matrix of weighted anomalies, X'. The matched filter estimates of **v** may then be easily calculated via regression with the first few principal components of X'.

$$\mathbf{m} = PC1\left(\mathbf{X}'\right) \qquad [3]$$

$$\hat{v} = b_o + \mathbf{b}^T\mathbf{m}, \forall i \in [1..n] \qquad [4]$$

MFR is computationally fast. This application applied an independent model to moving 0.5° windows across the ESEA region. Pacific Ocean SSTs (30°N-30°S, 130°E-80°W), Indian Ocean SSTs and precipitation (30°N-40°S, 30-120°E), and 200 and 500 hPa zonal and meridional winds over Africa (30°N-40°S, 0-90°E) were used as predictors.

4. Validation

4.a IRE Validation

The at-station accuracy of the FCLIM monthly long term mean were evaluated numerically by comparing the regression estimates at each of the 6965 points to the modeled value for each month. The error statistics were promising, with a coefficient of determination of 0.9, a mean bias error of 0.06 mm month[-1], and mean absolute error of 18 mm month[-1]. Figure 2, panel A shows the mean annual FCLIM precipitation and FAO climate normal locations for sub-Saharan Africa.

Three regional evaluations of the IRE methodology have been carried out for difficult modeling regions: Bhutan, Ethiopia, and western Kenya. These test sites were chosen because they represent dramatic rainfall estimation regimes for which independent station data sets were obtained through international collaboration. The validation studies correspond to a range of ancillary station data densities corresponding to no additional station data (Bhutan), modest additional station data resources (1 station per 10,000 km[2]) and dense station coverage (1 station per 1,800 km[2]).

For Bhutan, a very mountainous country (area~47,000 km[2]) in Southwest Asia (Figure 2.B), 20 stations were averaged each month from May of 2001 through December of 2003. These values are shown as blue triangles in Figure 2.C. Situated on the southern slopes of the Himalayas; rainfall is very heavy during the summer monsoon season, reaching values of greater than 500 mm month[-1]. Bhutan does not report on the Global Telecommunication System, and the NOAA Climate Prediction Center RFE values exhibit substantial bias (red columns in Figure 2.C). Unbiased RFE values derived using matched filter grids of monthly long term means are shown with blue columns. The UBRF adjustment (eq. 1) reduces the systematic bias to 4 mm month[-1], reduced the mean absolute error by 65% and resulted in a coefficient of determination (including the seasonal cycle) of 0.92. Note that the additional station data has *not* been included, since

the objective of this case study was to demonstrate the effectiveness of unbiasing using only long-term mean fields.

A more detailed cross-validation analysis for Ethiopia examined the at-station accuracies of the full IRE process. This validation calculated at-station statistics based on 11 years (1995-2005) of CPC ARC data and 120 National Meteorological Agency (NMA) station observations. For each month during the two main rainy seasons (Belg and Meher, March-September) a 10% random sample of stations was withheld and the full IRE estimation procedure (UBRF blended with stations) executed. For each of the 77 months (11 years x 7 months) the corresponding 0.1° pixel rainfall estimates were then extracted from the ARC and IRE grids and compared to the excluded stations.

Table 1 summarizes the at-station and pooled (regional) accuracy values. At a monthly/at-station scale the mean absolute error is high (42 mm) when compared to the long term mean average monthly rainfall of 112 mm month^{-1}. The IRE bias is low (~6 mm month^{-1}), however, and averaging in space reduces this value to 18 mm month^{-1} at the monthly time scale and 8 mm month^{-1} over a season. At-station monthly, regional monthly, and regional seasonal R^2 values are reasonably high (0.62, 0.8 and 0.82 respectively). The relative error values (MAE divided by temporal standard deviation) suggest useful signal to noise ratios; 0.43, 0.34 and 0.36 for the corresponding at-station monthly, regional monthly, and regional seasonal space-time scales. Figure 3 shows time-series of the averages of the excluded stations and the associated IRE pixel estimates. The fidelity is reassuring. Figure 4 shows the monthly bias and R^2 values of ARC and IRE estimates. ARC accuracy degrades later in the season, underestimating rainfall amounts and tracking poorly with observations, perhaps due to limitations associated with the cold cloud duration threshold.

A third detailed validation study was performed for a test site in Western Kenya (34.15°-35.55°E, 1°S-1°N). This site has been used in two previous evaluations: our accuracy assessment for the Collaborative Historical African Rainfall Model (CHARM, Funk et al., 2003) and a comparison between the CPC and NCAR-NCEP reanalysis fields (Funk and Verdin, 2003). A dense gauge network of 73 daily observations from 1961-1998 was interpolated to an 0.1° grid using inverse distance weighting. These 0.1° daily grids were accumulated to monthly totals and compared to the full IRE process driven by GPCP data.

Though coarse in resolution (2.5°) the GPCP data has the strong advantage of a climatological period of record (1979-2006, 28 years). The GPCP values were translated into ratios of the long term GPCP means and resampled using a cubic convolution to an 0.1° grid. These 0.1° ratios were multiplied against the corresponding FCLIM means, producing unbiased rainfall values. These UBRF fields were then merged with 19 stations drawn from the Global Historical Climate Network (Peterson and Vose, 1997).

The downscaled GPCP-based IRE fields recreate the long term mean structure of the region with a great deal of fidelity (Figure 5). The spatial R^2 of these fields is about 0.65 (Table 2) – which is impressive considering that the spatial footprint of the GPCP is

greater than the study site. The IRE values show no bias, and excellent temporal accuracies at the regional/seasonal scales ($R^2\sim0.87$). Even at the 0.1° monthly scale the mean absolute error (39 mm) is only 20% of the monthly mean of 175 mm, and about 54% of the monthly temporal standard deviation. This accuracy level (½ a standard deviation) is sufficient to capture extreme hydrologic variations. The monthly regional IRE averages track very well with high density gauge estimates (Figure 6).

4.b MFR forecast validation

Two metrics of forecast accuracy are examined here: forecast standard errors and regional comparisons for forecast and observed NDJ SPI values averaged over eastern southern Africa[3] and northeastern portions of the GHA[4]. Figure 7 shows the standard error values for OND, NDJ, and JFM. In November, a substantial basis for prediction exists, arising from persistent patterns in the Indian-Pacific SSTs and tropical circulations. Standard errors are typically less than ~0.6 SPI. This suggests a sufficient level of precision to capture the general magnitude and sign of climate anomalies several months in advance. Figure 8 shows average SPI time series for the eastern southern Africa and north-eastern Greater Horn regions. At this coarse regional scale agreement is fairly high. For eastern southern Africa non-El Niño droughts (1991/92, 1993/94) are captured well, as are the 2002/03 dry anomalies. The impacts of 1997/98 event are *not* over-estimated because the model responds more strongly to local conditions in the Indian Ocean. While the over all R^2 of the Greater Horn model is higher (0.76 vs. 071) more of this accuracy accrues from capturing the exceptional 1997/98 event, while modest wet seasons, such as 1992/93 are not captured effectively. In general, this region of Africa has more variance associated with persistent (~6 year) excursions. The forecasts represent this component quite well.

5. Application to the 2005/06 season for Kenya and Zimbabwe

The gray boxes in Figure 8 represent graphically the NDJ projections for the 2006/07 based on October 2006 reanalysis fields. The forecast for eastern southern Africa is -0.8 SPI ± 0.6, with a 68% chance of the observed SPI falling between -0.2 to -1.4 SPI. This suggests that below normal rainfall is quite likely. Given the current state (modest El Niño, positive Indian Ocean Dipole event, cold southwestern mid-latitude Indian Ocean) this forecast seems quite plausible. Visual inspection of the individual climate variables used to make our 2002/03 forecast[5] supports a pessimistic outlook for Southern Africa. The Greater Horn, on the other hand, will likely receive unseasonable heavy rains. The gray boxes in Figure 8 also show the forecast range for the eastern Greater Horn: +0.5 SPI ± 0.5, with a 68% chance of the observed SPI falling between 0 and 1.0 SPI. Figure 9 shows the spatial/seasonal distribution of OND, NDJ and DJF forecasts.

---

[3]Eastern southern Africa SPI based on eastern Botswana, southern Zambia, Zimbabwe, Southern Mozambique and northeastern South Africa.
[4] Greater Horn SPI based on Kenya, Somalia and the southern half of Ethiopia.
[5] ftp://hollywood.geog.ucsb.edu/pub/SA06/EvolvingOctoberAtNov5.ppt

6. Discussion and Conclusion

6.1 Discussion of the IRE validation studies

The IRE validation studies were selected to represent a selection of estimation scenarios corresponding to no additional station data (Bhutan), modest additional station data resources (1 station per 10,000 km^2) and dense station coverage (1 station per 1,800 km^2). Even with no station data, the UBRF procedure can enhance the accuracy satellite rainfall estimates, especially in areas with poor GTS coverage and complex terrain. Incorporating the UBRF enhances substantially the ability to correctly model the seasonal cycle and absolute magnitude of rainfall. Examination of the monthly bias and R^2 values for the Ethiopian case study (Figure 4) exhibit a similar seasonal dependence. Bias values are much lower and R^2 values are much higher early in the season. It appears likely that cold cloud duration rainfall metrics may have seasonal-latitudinal dependencies that can be largely accounted for by the UBRF process.

The seasonal-spatial UBRF correction may help explain the similar accuracy values obtained in the Ethiopian and Western Kenya accuracy assessments (Tables 1 and 2). A priori, one might expect the western Kenya accuracy statistics to be substantially higher than the Ethiopian results, given the much higher station density in the former study. At the regional scale the results are almost identical, bias ~0, relative error ~33%, and temporal R^2 values of ~0.8. It is also worth noting that in both cases seasonal and monthly accuracy levels were similar, implying perhaps that bias removal can substantially enhance our estimation accuracy at monthly time steps. For the monthly at-station and 0.1° scales similar results were again obtained with relative accuracies of ~½ a standard deviation. Given that the Ethiopia case corresponds to a typical national level monitoring capacity, it is quite encouraging that this level of accuracy can be obtained using modestly dense station data and the technically austere IRE techniques.

6.2 Discussion of the MFR forecast results

This study highlights the significance of the Indian Ocean SSTs and circulation features. While ENSO is a significant factor influencing African rainfall, many of these influences arise from lagged responses in the oceans and circulations surrounding the continent. Once the austral summer season has commenced, a fair level of climate persistence into the next few months supports statistical forecasts. The current climate state combines a modest El Niño with a modest positive dipole event. Past recent analogs to these events were 1982/83 and 1997/98 (Saji and Yamagata, 2003a). These combined events, referred to as 'nido' events (El Niño + IDO ~ nido) in Figure 8, were associated with extreme flooding in the Greater Horn (1997/98 not 1982/83) and drought in southern Africa (1982/83 not 1997/98). In general, the 1982/83 and 1997/98 events form reasonable brackets from about normal to very wet for the Greater Horn and about normal to very dry for Southern Africa. This is consistent with the MFR forecasts (Figures 8 & 9), although the forecasts results are more similar to 1982/83. In general, drought in Southern Africa might be more predictable than extreme flooding in eastern Africa. New research has associated extreme wet/dry events in southern Africa with the temperature

gradient between the western tropical and western sub-tropical Indian Ocean (Washington and Preston, 2006). This gradient is strongly was strongly present in October of 1982, October of 1997 and October of 2006. Below normal rains in Southern Africa seem likely, and extreme wetness in the Greater Horn possible.

6.3 Conclusion

The world was unprepared when persistent multi-year drought struck Africa in the 1970s, and this drought was responsible for 100,000 deaths in the Sahel and 200,000 deaths in Ethiopia. Following drought in 1983-1985 saw deaths in Ethiopia estimated from 400,000 to 1 million people. These large-scale famines shocked the world and pointed up the tragic lack of timely information. The past 20 years have seen a gradual accumulation of data, techniques modeling and remote sensing resources. Reasonable precipitation estimates and forecasts, using fairly simple statistical estimation procedures are now feasible. These procedures rely on locally systematic relationships between topography and larger scale precipitation patterns (IRE estimates) or local rainfall and synoptic circulation features (MFR forecasts). Both techniques benefit substantially from satellite-based observation/assimilation systems: satellite rainfall estimates and reanalysis climate fields. By leveraging the information contained in these products, and integrating forecast and hydro-climatic monitoring tools, we can effectively anticipate at least the sign if not the magnitude of hydro-climatic shocks in eastern and southern Africa.

References

Adler, R.F., G.J. Huffman, A. Chang, R. Ferraro, P. Xie, J. Janowiak, B. Rudolf, U. Schneider, S. Curtis, D. Bolvin, A. Gruber, J. Susskind, and P. Arkin, 2003: The Version 2 Global Precipitation Climatology Project (GPCP) Monthly Precipitation Analysis (1979-Present). J. Hydrometeor., 4,1147-1167.

FAO Agrometeorology Group. 2001. FAOCLIM 2.01 Worldwide Agroclimatic Database [CD-ROM]. Food and Agricultural Organization of the United Nations (FAO), Rome.

Funk C., Theiler J., Roberts, D., Borel C. (2001): Clustering to Improve Matched Filter Detection of Weak Gas Plumes, in Hyperspectral Thermal Imagery, *IEEE Transactions on Geoscience and Remote Sensing.* **V39.7** 1410-1419. August 6th-7th, 2001.

Funk, C., T. Magadazire, G. Husak, J. Verdin, J. Michaelsen, and J. Rowland, 2002: Forecasts of 2002/2003 Southern Africa Maize Growing Conditions Based on October 2002 Sea Surface Temperature and Climate Fields. FEWS NET Special Report. December, 2002.

Funk, C., J. Michaelsen, J. Verdin, G. Artan, G. Husak, G. Senay, H. Gadain, and T. Magadazire, 2003: The Collaborative Historical African Rainfall Model: Description and Evaluation. *International Journal of Climatology*, **23,** 47-66

Funk, C. and Michaelsen, J., 2004: A simplified diagnostic model of orographic rainfall for enhancing satellite-based rainfall estimates in data poor regions. Journal of Applied Meteorology, V34. 1366-1378

Grimes, D.I.F., Pardo-Iguzquiza, E. and Bonifacio, R., 1999. Optimal areal rainfall estimation using raingauges and satellite data. Journal of Hydrology, 222: 93-108.

Huffman, G.J., R.F. Adler, B. Rudolph, U. Schneider, and P. Keehn, 1995: "Global Precipitation Estimates Based on a Technique for Combining Satellite-Based Estimates, Rain Gauge Analysis, and NWP Model Precipitation Information", J. Clim., 8, 1284-1295.

Huffman, G.J., R.F. Adler, P. Arkin, A. Chang, R. Ferraro, A. Gruber, J. Janowiak, A. McNab, B. Rudolph, and U. Schneider, 1997: "The Global Precipitation Climatology Project (GPCP) Combined Precipitation Dataset", Bul. Amer. Meteor. Soc., 78, 5-20.\

Husak, GJ, Michaelsen J, Funk C. 2006. Use of the Gamma Distribution to Represent Monthly Rainfall in Africa for Drought Monitoring Applications. International Journal of Climatology, In Press.

Janowiak, J.E., Gruber, A., Kondragunta, C.R., Livezey, R.E. and others., a., 1998. A comparison of the NCEP-NCAR reanalysis precipitation and the GPCP rain gauge-satellite combined dataset with observational error considerations. Journal of Climate, 11(11): 2960-79.

Kates, R. W., 2000: Cautionary Tales: Adaptation and the Global Poor. Climatic Change, 45, 5-17.

Landman, W.A. & Goddard, L. (2002). Statistical recalibration of GCM forecasts over southern Africa using model output statistics. Journal of Climate, 15(15): 2038-2055.

McHugh, M. J., 2004: Near-surface zonal flow and East African precipitation receipt during Austral summer. *Journal of Climate*, **17**, 4070-4079.

McKee, T. B., N. J. Doesken, et al. (1993). The Relationship of Drought Frequency and Duration to Time Scales. 8th Conference on Applied Climatology.

McKee, T. B., N. J. Doesken, et al. (1994). Drought Monitoring with Multiple Time Scales. 9th Conference on Applied Climatology.

New, M., Hulme, M. and Jones, P., 1999. Representing twentieth-century space-time climate variability. I. Development of a 1961-90 mean monthly terrestrial climatology. Journal of Climate, 12(3): 829-56.

New, M., Hulme, M. and Jones, P., 2000. Representing twentieth-century space-time climate

variability. II. Development of 1901-96 monthly grids of terrestrial surface climate. Journal of Climate, 13(13): 2217-38.

Peterson, T.C. and Vose, R.S.V., 1997. An overview of the Global Historical Climatology Network temperature data base. Bulletin of the American Meteorological Society, 78: 2837-2849.

Peterson, T. C. and R. S. Vose, 1997: An overview of the Global Historical Climatology Network temperature data base. Bull. Amer. Meteor. Soc., 78, 2837-2849. Queney, P., 1948. The problem of air flow over mountains: a summary of theoretical studies. Bulletin of the American Meteorological Society, 29: 16-25.

Rockstrom, J., 2000. Water Resources Management in Smallholder Farms in Eastern and Southern Africa: An Overview. Phis. Chem. Earth (B), 25(3): 275-283.

Saji, N. H. and T. Yamagata, 2003: Structure of SST and surface wind variability during Indian Ocean dipole mode events: COADS observations. *Journal of Climate*, **16**, 2735-2751.

N. H. Saji, T. Yamagata; Possible impacts of Indian Ocean Dipole mode events on global climate, *Climate Research*, Vol. 25: 151-169, 2003

R. Washington, A. Preston, 2006. Extreme wet years over southern Africa: Role of Indian Ocean sea surface temperatures, J. of Geophysical Res., 111(D15104).

Willmott, C.J. and Feddema, J.J., 1994. Estimating continental and terrestrial precipitation averages from rain-gauge networks. International Journal of Climatolgy, 14(4): 403-414.

Willmott, C.J. and Matsura, K., 1995. Smart Interpolation of Annually Averaged Air Temperature in the United States. Journal of Applied Meteorology, 34: 2577-2586.

Willmott, C.J. and Robeson, S.M., 1995. Climatologicall Aided Interpolation (CAI) of Terrestrial Air Temperature. International Journal of Climatolgy, 15(2): 221-229.

Wilks D. 1990. Maximum Likelihood Estimation for the Gamma Distribution Using Data Containing Zeros. Journal of Climate 3: 1495-1501.

Wilkes, D.S., 1995. Statistical methods in the atmospheric sciences. Academic Press, 467 pp.

Xie, P. and Arkin, P.A., 1997. Global Precipitation: A 17-Year Monthly Analysis Based on Gauge Observations, Satellite Estimates and Numerical Model Outputs. Bulletin of the American Meteorological Society, 78(11): 2539-2558.

Xie, P. and Arkin, P.A., 1998. Global monthly precipitation estimates from satellite-observed outgoing longwave radiation. Journal of Climate, 11(2): 137-64.

Xie, P., Yarosh, Y., Love, T., Janowiak, J. & Arkin, P.A., (2002). A real-time daily precipitation analysis over South Asia, 16th Conference on Hydrology. American Meteorological Society, Orlando, FL.

Tables

Table 1. Ethiopian test site evaluation statistics. The March-September and Monthly rows report statistics for the seasonal March-September and individual monthly March-September accumulations, respectively. The first and second columns report mean bias and mean absolute errors based on the average of all stations. The MAE STD^{-1} column provides a relative metric of uncertainty, with typical errors being about ~33% of the temporal standard deviation. The time R^2 is calculated using 11 years of data (1995-2005). The last three columns are similar to the regional metrics, but based on calculations using the individual station values. Seasonal at-station values were not available do to the random sampling associated with the cross-validation.

IRE	Regional Metrics				At-station metrics		
	MBE	MAE	MAE STD^{-1}	Time R^2	MAE	MAE STD^{-1}	Time R^2
Seasonal	6	8	0.36	0.82	---	---	---
Monthly	6	18	0.34	0.80	42	0.43	0.62

Table 2. Kenya test site evaluation statistics. The MAM and Monthly rows report statistics for the seasonal March-May and individual March-April-May accumulations, respectively. The first column reports the R^2 of the long term (1979-2005) averages at the 294 (14 rows x 21 columns) 0.1° pixels. The second and third columns report mean bias and mean absolute errors based on the average of all 294 pixels. MAE and MBE are reported in mm month^{-1}. The MAE STD^{-1} column provides a relative metric of uncertainty, with typical errors being about ~33% of the temporal standard deviation. The time R^2 is calculated using 27 years of data (1979-2005). The last three columns are similar to the regional metrics, but based on calculations using the individual 0.1° values.

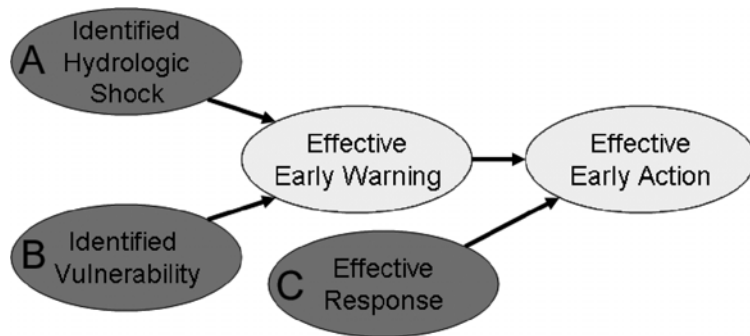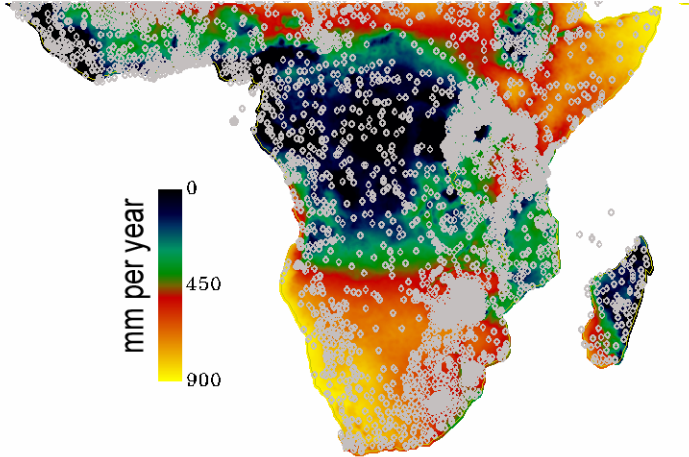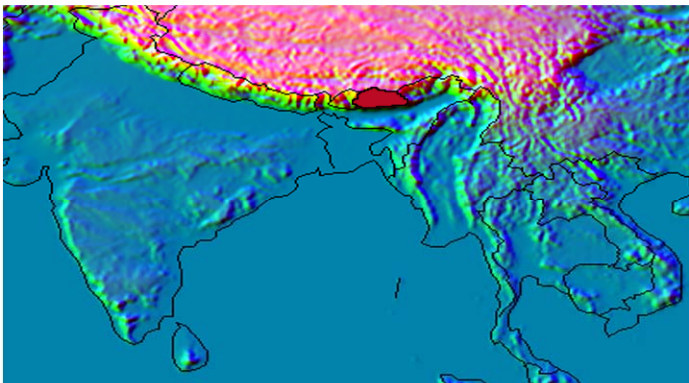|	Regional Metrics					At-pixel metrics		
	Spatial R^2	MBE	MAE	MAE STD^{-1}	Time R^2	MAE	MAE STD^{-1}	Time R^2
Seasonal	0.67	0.01	8	0.31	0.87	26	0.52	0.54
Monthly	0.64	0.00	14	0.37	0.75	39	0.54	0.49

Figures

Figure 1. Hydrologic Early Warning Schema

A. Annual FCLIM Average Precipitation and FAO climate normal locations for sub-Saharan Africa
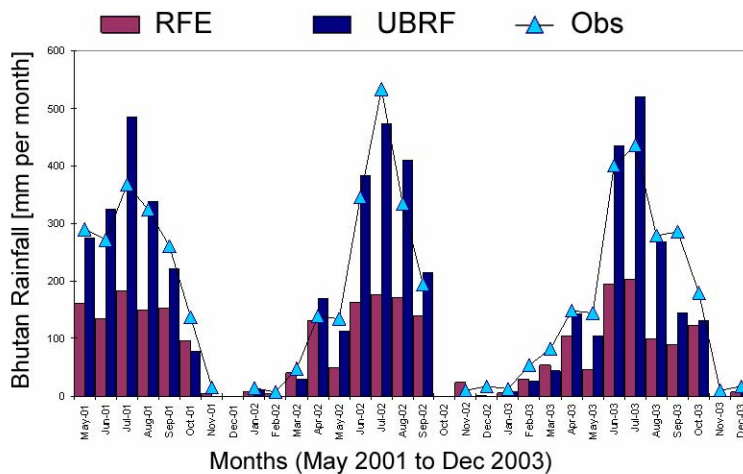
Figure 2. Panel A displays FCLIM annual means and FA0CLIM 2.0 station locations for sub-Saharan Africa. Panel B shows GTOPO030 elevation, east-west and north-south slopes mapped to red green and blue shading. The red polygon identifies Bhutan. Panel C shows monthly mean RFE, UBRF and Observed rainfall for Bhutan.
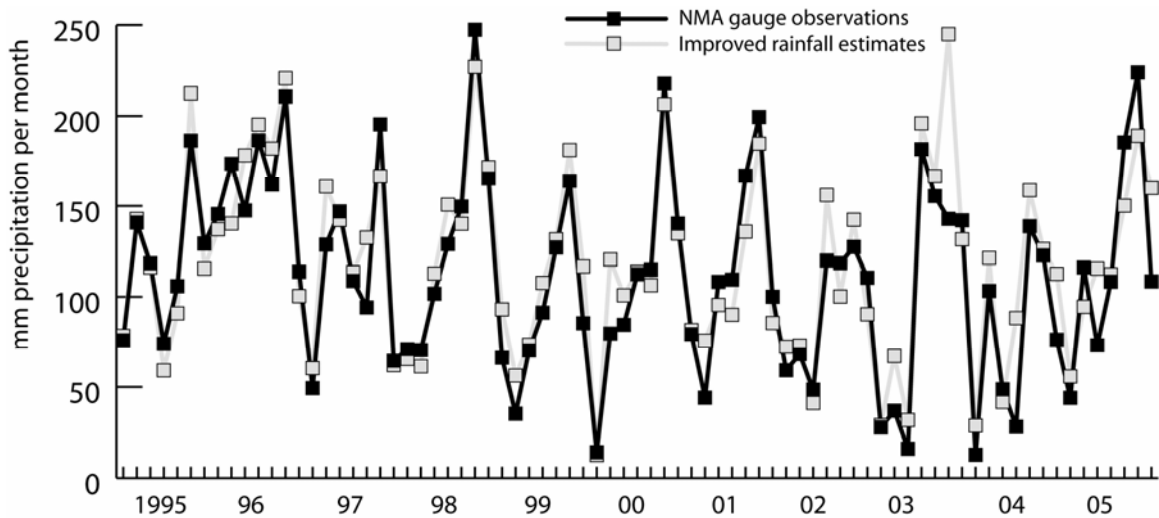
B. Elevation, east-west and north-south slope mapped to red, green, blue for Southeast Asia.

C. CPC RFE, Unbiased Rainfall and station observations for Bhutan

Figure 3. Ethiopian observed and cross-validated monthly averages. Each observed datum is based on the average of a 10% sample of the NMA gauge network. The corresponding 0.1° IRE pixels were also averaged and plotted. The seven months of the main growing seasons (March-September) are shown.
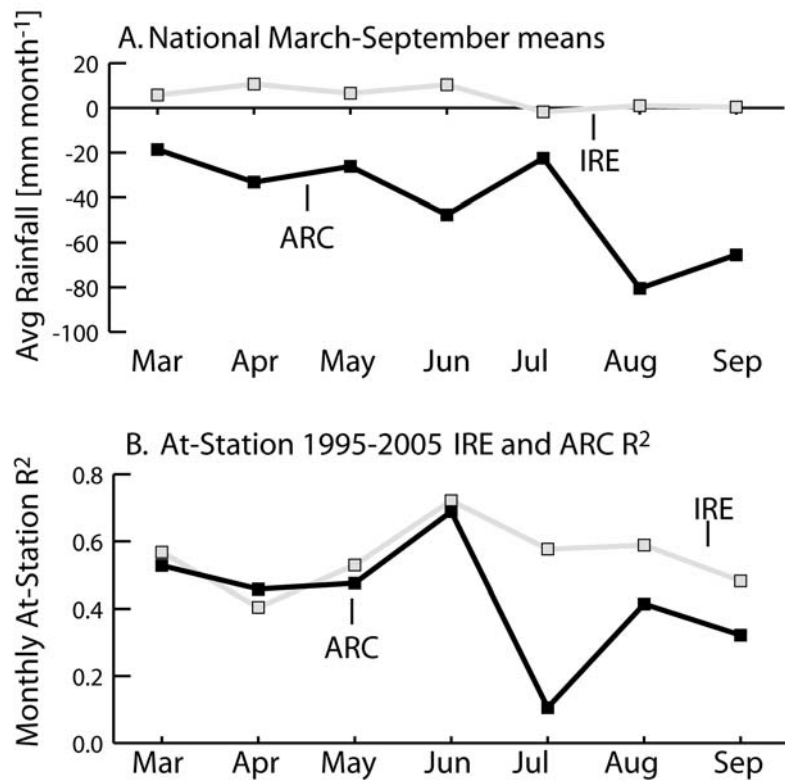
Figure 4. Monthly rainfall bias and R^2 values for the Ethiopian test site.
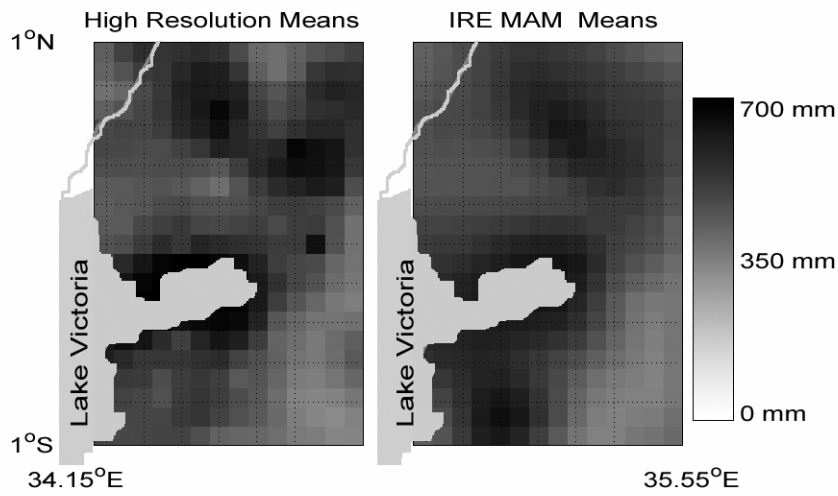
High Resolution Means   IRE MAM Means

Figure 5. 1979-2005 mean March-April-May rainfall over the western Kenya test site.
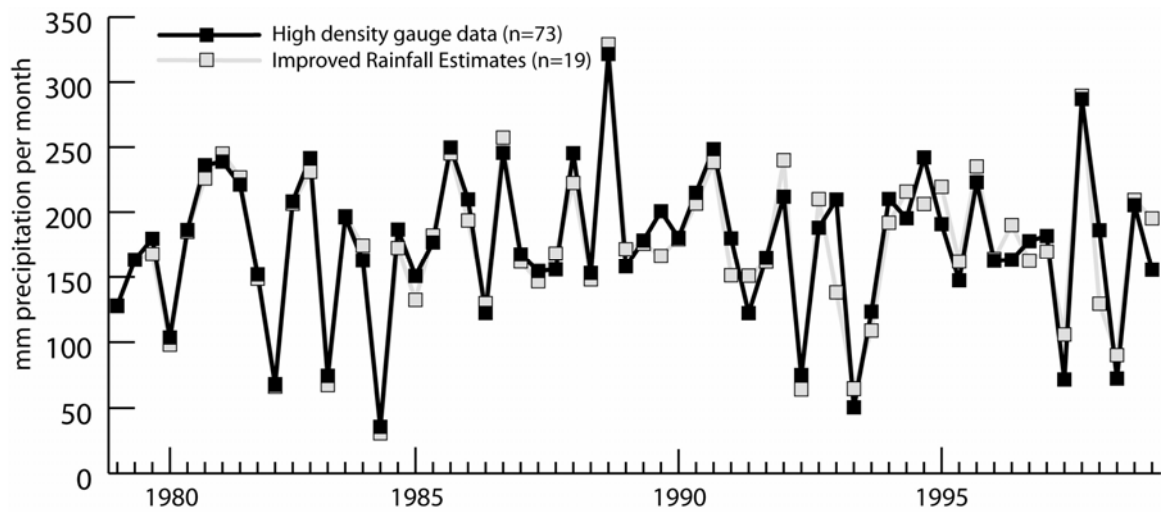
Figure 6. Monthly mean 1979-2005 high density gauge and improved rainfall estimates over the Kenya test site.
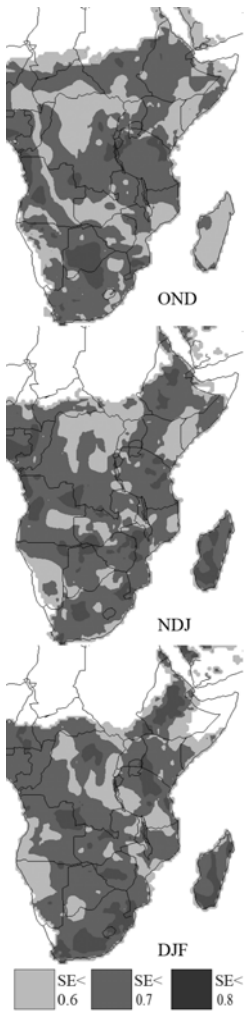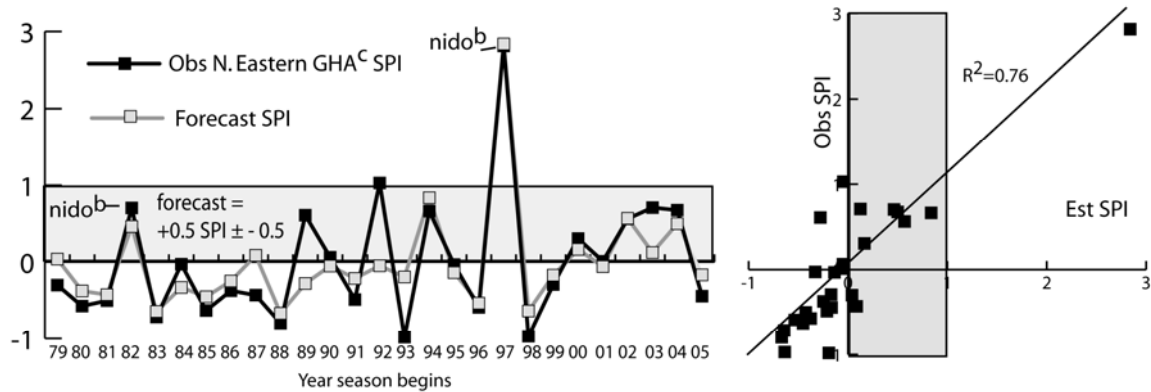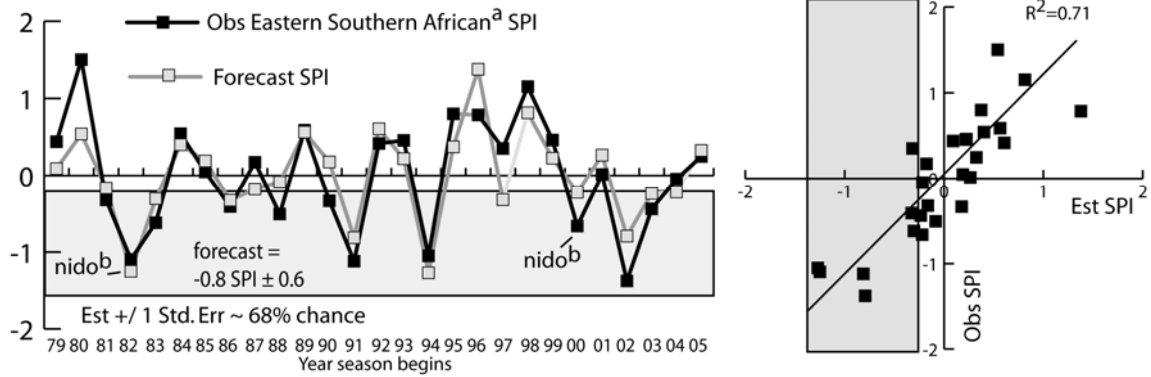
Figure 7. Standard errors associated with the OND, NDJ and DJF forecasts over the 1979-2005 time period.

a Eastern Southern Africa SPI based on eastern Botswana, southern Zambia, Zimbabwe, Southern
  Mozambique and northeastern South Africa
b 'nido' refers to El Nino-positive Indian Ocean Dipole years
c Northeast Greater Horn SPI based on Kenya, Somalia and the southern half of Ethiopia

Figure 8. Regional observed and forecast NDJ SPI values. Light gray boxes display likely range of the 2006 forecast, based on October reanalysis data. R^2 of GHA without the 1997-98 event is 0.55.
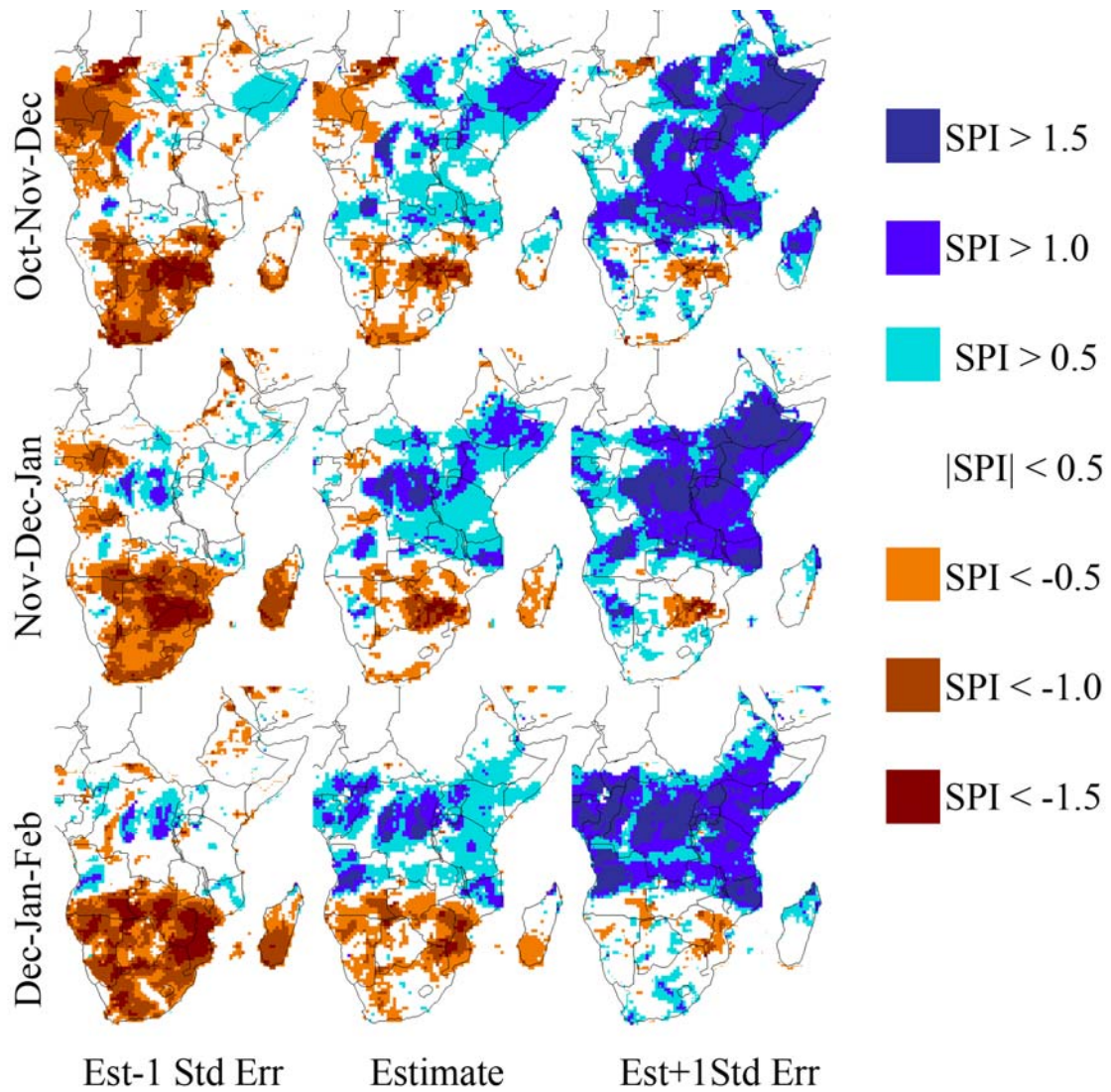
Figure 9. Maximum likelihood and ±1 standard error MFR forecasts for OND, NDJ and JFM.